ADVANCED ENERGY & SUSTAINABILITY RESEARCH
www.advenergysustres.com

Low-Carbon Poly(3-vinyl-*N*-methylphenothiazine) Electrode Formulation Using PEDOT:PSS (poly (3,4-ethylenedioxythiophene):poly(styrene sulfonate)) for Lithium-Based Energy Storage

*Sathiya Priya Panjalingam, Philipp Penert, Birgit Esser, Martin Winter, and Peter Bieker**

Metal-free organic electrode materials are of increasing interest due to their environmental compatibility, natural abundance, and structural versatility. Poly(3,4-ethylenedioxythiophene):poly(styrene sulfonate) (PEDOT:PSS) is an intrinsically conductive polymeric salt that has emerged as a multifunctional electrode material, serving both as a conductive additive and as binder in energy storage applications. Organic electrode materials´ inherent low electronic conductivity often necessitates high loadings of conductive carbon additives, which diminishes the overall energy density. To overcome this challenge, PEDOT:PSS is investigated as a partial substitute for traditional conductive carbon in poly(3-vinyl-*N*-methylphenothiazine) (PVMPT) redox polymer electrodes. Remarkably, even with a high PVMPT content of 80 wt% and a reduced carbon content to 15 wt%, the composite electrode delivers a reversible capacity of 84 mAh g^{-1}, which is ≈81% of that achieved with 50 wt% PVMPT and 45 wt% carbon black, over 250 cycles at 1C rate. Importantly, the fabrication process employs water-based processing with a carboxymethyl cellulose (CMC) binder, completely avoiding hazardous solvents such as *N*-methyl-2-pyrrolidone (NMP) and polyvinylidene difluoride (PVdF) binder. Overall, these results highlight the potential of PEDOT:PSS to enable low-carbon content, high-performance, and eco-friendly organic battery electrodes that align with the principles of sustainable energy storage.

1. Introduction

The intensifying global demand for lithium ion batteries (LIBs), driven by the rapid expansion of electric vehicles and portable electronics, has increased the consumption of critical minerals, such as lithium, cobalt, and nickel, essential components of LIB positive electrode materials.[1–4] While advancements in battery chemistry and end-of-life management offer potential solutions for meeting future energy needs, the reliance on scarce, nonrenewable resources raises pressing sustainability concerns. The energy-intensive extraction and the manufacturing processes of these raw materials contribute to a high environmental burden. These challenges are further exacerbated by potential mismatches between supply and demand, leading to price volatility and heightened ecological impacts. As a result, the pursuit of sustainable alternatives has become a top priority.[5–7]

In this regard, transition metal-free organic electrode materials are commendable for their enhanced electrochemical performance and environmentally friendly nature, aligning well with sustainability objectives such as reduced costs, renewable sources, and less energy-intensive end-of-life processing compared to traditional inorganic materials.[5,8–10] Their structural versatility also supports both n-type and p-type charge storage, enabling a variety of cell configurations.[8,11–13] However,

S. Priya Panjalingam, M. Winter, P. Bieker
MEET Battery Research Center
Institute of Physical Chemistry
University of Münster
Corrensstr. 46, 48149 Münster, Germany
E-mail: peter.bieker@fz-juelich.de

The ORCID identification number(s) for the author(s) of this article can be found under https://doi.org/10.1002/aesr.202500428.

© 2025 The Author(s). Advanced Energy and Sustainability Research published by Wiley-VCH GmbH. This is an open access article under the terms of the Creative Commons Attribution License, which permits use, distribution and reproduction in any medium, provided the original work is properly cited.

DOI: 10.1002/aesr.202500428

S. Priya Panjalingam
International Graduate School for Battery Chemistry Characterization Analysis Recycling and Application (BACCARA)
University of Münster
Corrensstr. 40, 48149 Münster, Germany

P. Penert, B. Esser
Institute of Organic Chemistry II and Advanced Materials
Ulm University
Albert-Einstein-Allee 11, 89081 Ulm, Germany

M. Winter, P. Bieker
Helmholtz Institute Münster (HI MS), IMD-4
Forschungszentrum Jülich Gmbh
University of Münster
Corrensstr. 46, 48149 Münster, Germany

a key challenge associated with these materials is their inherently low electronic conductivity, necessitating the incorporation of substantial amounts of conductive additives. Another major obstacle is the dissolution of small organic molecules in electrolytes. This issue can be mitigated through approaches such as salification, the integration of porous conductive materials, electrolyte optimization, and polymerization.[14–16] The former challenge, low electronic conductivity, can be addressed using specialized conductive additives, a strategy that remains relatively unexplored. Some studies have explored the use of specialized conductive carbons, either as an added conductive additive or as an in situ coating during synthesis, which reduces the required carbon content while enhancing conductivity.[17–20]

A conducting polymer from the polythiophene family, poly (3,4-ethylenedioxythiophene): poly(styrenesulfonate) (PEDOT:PSS), has garnered considerable attention due to its low toxicity and water solubility, enabling eco-friendly aqueous processing, high electronic conductivity, and good electrochemical stability up to 4.2 V. In addition, it offers favorable thermal, chemical, and mechanical properties, making it well-suited for enhancing electrode performance.[21–23] The electrical conductivity of PEDOT:PSS ranges from 6.23×10^{-2} to $4.2\ \mathrm{S\,cm^{-1}}$ depending on the processing conditions.[22,24,25] Conductivity can be further improved by introducing secondary dopants, such as formic acid.[22] This high electronic conductivity stems from the delocalization of holes along the doped PEDOT backbone, enabling efficient charge transport, and the positive charges in doped PEDOT are stabilized by PSS dopant.[22,25] Thanks to its high electronic conductivity, PEDOT:PSS is a viable replacement for conventional conductive materials like carbon black.[21,22,26] PEDOT, composed of π-conjugated 3,5-ethylenedioxythiophene units, carries positive charges, that are balanced by the dissociated sulfonate anions in PSS, forming a stable ionic complex.[17] PSS acts as a polymeric surfactant, aiding in the proper dispersion and stabilization of PEDOT in aqueous solutions. It also imparts good mechanical flexibility and strong adhesion, making PEDOT:PSS an effective binder. It readily forms uniform, thin films over the active material particles, ensuring good contact with a current collector.[21] It has been employed in both inorganic and organic electrodes, demonstrating multifunctional properties.[17,21,22,27,28] For instance, Ma et al. used PEDOT:PSS as a multifunctional binder in a sulfur-heterocyclic quinone positive electrode DTT (dibenzo[b,i]thianthrene-5,7,12,14 tetraone), where it effectively reduced active material dissolution and improved electrochemical performance.[17] More recently, Kato et al. demonstrated that a PEDOT:PSS-coated separator can extend battery cycle life by preventing the dissolution of the indigo-based organic electrode. This strategy enabled access to 96% of the theoretical capacity ($204\ \mathrm{mAh\,g^{-1}}$) with an active material content of 80 wt%.[28]

The present work investigates the influence of PEDOT:PSS on the electrochemical performance of PVMPT-based positive electrodes. PVMPT is a p-type, nonconjugated heterocyclic redox polymer, incorporating phenothiazine redox moieties as pendants of an aliphatic polymer backbone. This material exhibits excellent cycle life, high-rate capability, a moderate theoretical specific capacity of $112\ \mathrm{mAh\,g^{-1}}$ (assuming a one-electron redox process), and a discharge potential of 3.5 V versus Li|Li^+.[29–31] The charge–discharge mechanism and the solubility of the oxidized state of PVMPT have been extensively studied and documented using various strategies, including electrolyte optimization, the use of highly porous conductive additives, and the development of composite electrodes incorporating specialized conductive additives.[15,16,29,30,32] This study focuses on minimizing the use of conventional carbon additives by introducing PEDOT:PSS as an additional conductive component. Electrodes were fabricated with a high active material content (80 wt% PVMPT) and 20 wt% total inactive materials, including conductive additive, PEDOT:PSS, and binder. Morphological and electrochemical characteristics were examined using scanning electron microscopy and galvanostatic cycling investigations. The results demonstrate that an optimized combination of PEDOT:PSS and conductive additive enhances electrical conductivity, improves accessible capacity with high content of active material, supporting the development of high-performance organic materials.

2. Experimental Section

2.1. Synthesis of PVMPT

PVMPT was synthesized as previously reported.[29,30]

2.2. Electrode Production and Processing

Electrodes were fabricated by blending the synthesized PVMPT powder with a commercially available conductive additive, carbon black (CB) (Super C65, Imerys Graphite & Carbon), along with sodium carboxymethyl cellulose (Na-CMC, CRT 2000 PPA12, Dow Wolff Cellulosics, Germany) as binder and PEDOT:PSS (dry re-dispersible pellets, Sigma Aldrich). The pellets were re-dispersed in water to prepare the aqueous solution used during electrode fabrication. The supplier does not provide the electrical conductivity of the PEDOT:PSS, but instead reports a sheet resistance of 200–450 $\Omega\ \mathrm{sq^{-1}}$. The electrode pastes were prepared using a Thinky mixer, incorporating PVMPT, CB, PEDOT:PSS, and Na-CMC. The composition consisted of 80 wt% PVMPT and 5 wt% Na-CMC, while the weight ratios of CB and PEDOT:PSS were varied. To ensure homogeneous mixing, CMC and PEDOT:PSS solutions were stirred overnight using a magnetic stirrer before being used in electrode paste preparation. A reference electrode paste was also prepared without the addition of PEDOT:PSS, comprising 80 wt% PVMPT, 15 wt% CB, and 5 wt% Na-CMC, which is referred to as 0 wt% PEDOT:PSS.

For the reference sample with 0 wt% PEDOT:PSS, PVMPT, and CB were first ground together using a mortar and pestle for 10 min. Subsequently, the Na-CMC binder solution and the required amount of water were added. Once the desired consistency was achieved, the mixture was transferred to the Thinky mixer and mixed at 1700 rpm for 1 h. For samples containing PEDOT:PSS, the processing method was slightly modified. First, the Na-CMC binder solution and PEDOT:PSS solution were homogenized. CB was then added and mixed at 1700 rpm for 30 min. PVMPT was subsequently introduced into the mixture and pre-ground using a mortar and pestle for 10 min. Final mixing was carried out in the Thinky mixer at

© 2025 The Author(s). Advanced Energy and Sustainability Research published by Wiley-VCH GmbH

26999412, 2026, 3, Downloaded from https://advanced.onlinelibrary.wiley.com/doi/10.1002/aesr.202500428 by Karlsruher Institut Fur Technologie, Wiley Online Library on [01/11/2026]. See the Terms and Conditions (https://onlinelibrary.wiley.com/terms-and-conditions) on Wiley Online Library for rules of use; OA articles are governed by the applicable Creative Commons License

Table 1. Weight percentage(composition) of the electrode components.

Formulation	PVMPT	CB	PEDOT:PSS	CMC
0 wt% PEDOT:PSS	80	15	0	5
5 wt% PEDOT:PSS	80	10	5	5
7.5 wt% PEDOT:PSS	80	7.5	7.5	5
10 wt% PEDOT:PSS	80	5	10	5

1700 rpm for 30 min to ensure uniform dispersion. Electrode compositions, listed by weight percentage, and their assigned reference notations are detailed in **Table 1**.

The prepared electrode pastes were spread onto 5 wt% KOH-etched aluminum foil (Speira, thickness: 20 µm) using the doctor-blade (Zehntner 4-sided film applicator) method (50 µm spacing). The electrodes underwent a two-step drying process: primary drying in a hot air oven for 1 h, followed by secondary drying in a vacuum drying cabinet at 70 °C overnight. Electrode discs (12 mm in diameter) were then prepared, densified at 3 ton pressure using a hydraulic press for 20 s, and further dried under reduced pressure (0.005 mbar) in a Büchi B-585 glass oven at 120 °C for 12 h. The final electrodes exhibited dry film thicknesses of 10–13 µm (excluding the current collector), and the active mass loading was between 0.44 and 0.5 mg cm^{-1}.

2.3. Cell Assembly and Electrochemical Measurements

The electrochemical performance was evaluated using a three-electrode Swagelok T-Cell setup. Half-cells were assembled with lithium metal serving as both the counter (12 mm disc) and reference electrode (5 mm disc), while PVMPT composite electrodes were used as the working electrode. All cells were assembled in a dry room with humidity levels maintained below 20 ppm. After assembly, the cells were allowed to rest for 12 h before cycling. The electrolyte used for the measurements was 1.0 M $LiPF_6$ in 3:7 EC: EMC v/v (Solvionics, 99.9% H_20: 20 ppm max). Six layers of Freudenberg 2190 nonwoven polypropylene separator (FS-2190) were soaked with 130 µL electrolyte for the counter electrode and the working electrode (13 mm separator) while 60 µL (10 mm separator) at the reference electrode. The separators were punched and pre-dried under reduced pressure (0.005 mbar) at 120 °C for 24 h in Büchi B-585 glass oven before cell assembly. The molecular sieves activated at 300 °C for 24 h under reduced pressure were used to dry the electrolyte prior to use for the cell assembly. Galvanostatic cycling investigations were performed using a MACCOR 4000 series battery tester at various C-rates, as specified in the corresponding figure captions. Cyclic voltammetry was performed with Swagelok T-cells using a Biologic (VMP3 Potentiostat) Science Instruments at 20 °C in a Binder oven between the voltage window of 3.0 to 4.0 V.

3. Physical Characterization

3.1. Scanning Electon Microscopy (SEM)

SEM micrographs of the PVMPT polymer powder and PVMPT composite electrodes (pristine) were obtained using a Carl Zeiss AURIGA Crossbeam Workstation. The imaging was performed at an accelerating voltage of 3 kV with an in-lens detector, maintaining a working distance of 4 mm.

Cross-sectional samples were prepared using a cooling cross-section polisher (IB-19520CCP, Jeol). The milling process included an initial coarse step at 5 kV with an argon flow rate of 2.0 for 2.5 h at a width of 100 µm, followed by a fine milling at 2 kV with an argon flow rate of 9.0 for 1 h. SEM images were obtained on a Zeiss Crossbeam 550 electron microscope (Carl Zeiss Microscopy GmbH) at accelerating voltage of 3 kV using an in-lens detector at a working distance of 5 mm. For energy-dispersive X-ray spectroscopy (EDS) analysis, an Ultim Extreme detector was used to evaluate the elemental composition of the electrodes at accelerating voltage of 5 kV at a working distance of 5 mm.

4. Results and Discussion

The chemical structures of PVMPT, CMC, and PEDOT:PSS are depicted in **Figure 1**, with the redox-active phenothiazine moiety highlighted in the gray dotted box.

4.1. Characterization and Electrochemical Analysis of Low-Carbon Electrodes Formulated with CMC and PEDOT:PSS

Figure 2 illustrates the potential versus capacity profiles of electrodes prepared without PEDOT:PSS, as well as those with varying weight ratios of PEDOT:PSS and CB, recorded at the 1st,

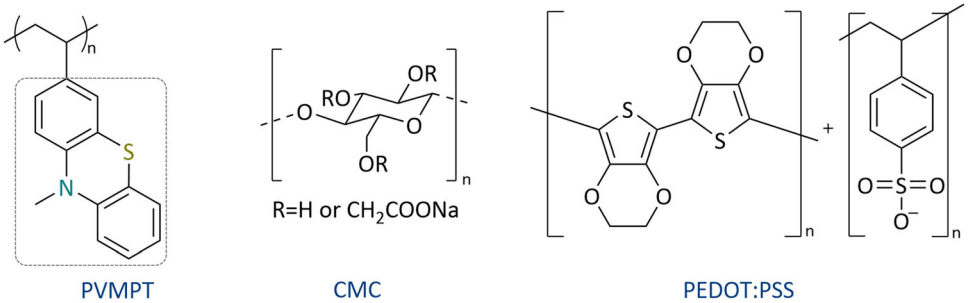


Figure 1. Chemical structure of PVMPT, with the phenothiazine redox moiety highlighted by the gray dotted box, along with the binders–CMC and PEDOT:PSS.

© 2025 The Author(s). Advanced Energy and Sustainability Research published by Wiley-VCH GmbH

26999412, 2026, 3, Downloaded from https://advanced.onlinelibrary.wiley.com/doi/10.1002/aesr.202500428 by Karlsruher Institut Fur Technologie, Wiley Online Library on [01/11/2026]. See the Terms and Conditions (https://onlinelibrary.wiley.com/terms-and-conditions) on Wiley Online Library for rules of use; OA articles are governed by the applicable Creative Commons License

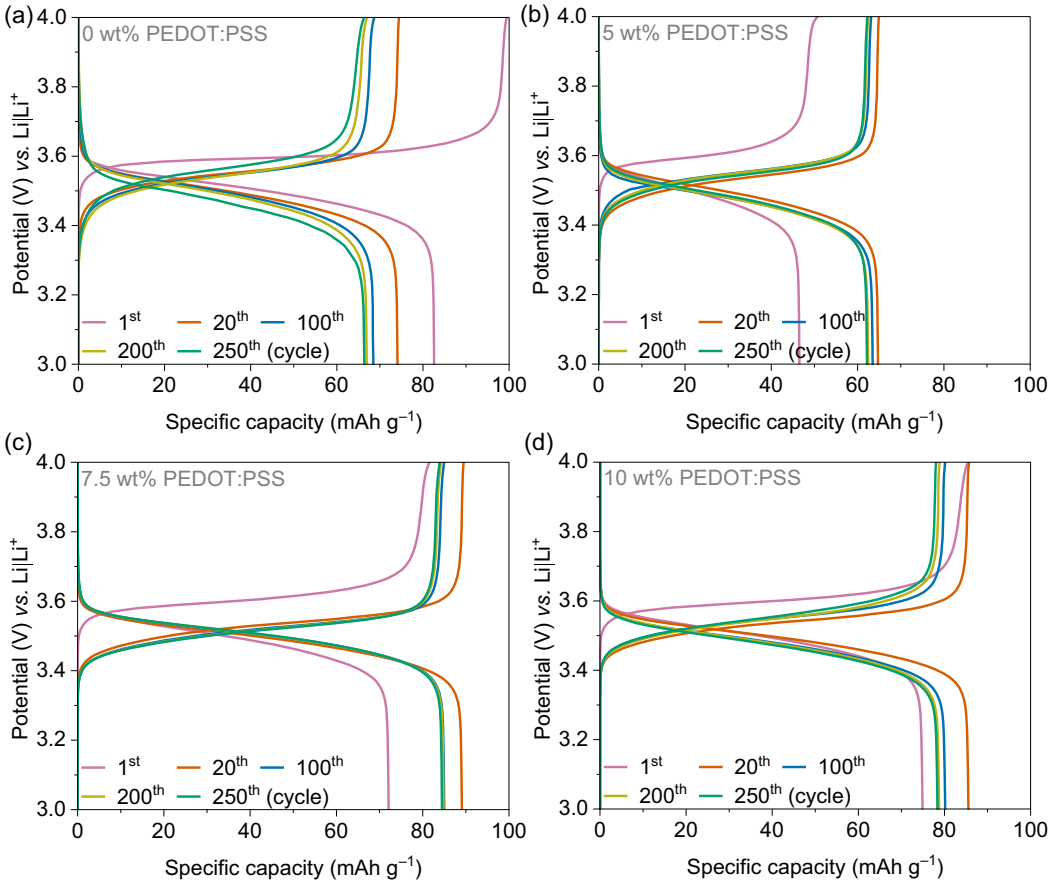


Figure 2. Potential versus capacity profiles for selected cycles of cells operated at a 1C rate, comparing electrodes without PEDOT:PSS to those containing PEDOT:PSS at three different weight percentages: a) 0 wt% PEDOT:PSS, b) 5 wt% PEDOT:PSS, c) 7.5 wt% PEDOT:PSS, and d) 10 wt% PEDOT:PSS.

20th, 100th, 200th, and 250th cycles. Figure 2a presents the electrode formulated without PEDOT:PSS. In this case, the initial specific discharge capacity reaches 82 mAh g^{-1}, which gradually declines with cycling, reaching 66 mAh g^{-1} by the end of 250th cycle. This behavior differs slightly from previously reported results. Kolek et al. demonstrated the trend of high initial capacity followed by a decline, which was attributed to the polymer structural reorganization during anion (de)insertion, and then a subsequent increase to a maximum capacity.[15,29,30] Notably, that study used electrodes with 45 wt% CB. By contrast, the formulation used herein for 0 wt% PEDOT:PSS electrodes includes 80 wt% PVMPT, 15 wt% CB, and 5 wt% CMC. Although increasing the proportion of active material while reducing the CB content does not alter the charge–discharge mechanism entirely, it prevents the capacity enhancement after certain cycles as observed in prior studies. This limitation arises from the inherently low conductivity of PVMPT and the reduced CB content, which together yield a poorly conducting electrode that prevents the capacity increase after the initial decline caused by polymer restructuring process.

With the increase in PEDOT:PSS content from 5 to 10 wt%, a noticeable variation in cycling behavior is observed. Figure 2b presents the potential versus capacity profile for the electrode containing 5 wt% PEDOT:PSS. The initial discharge capacity is 47 mAh g^{-1}, which increases to 65 mAh g^{-1} by the 20th cycle, followed by a gradual decline to 60 mAh g^{-1}. A similar trend is observed for all electrodes incorporating PEDOT:PSS (7.5 wt% and 10 wt% PEDOT:PSS electrodes). As shown in Figure 2c, the electrode with 7.5 wt% PEDOT:PSS displays an initial discharge capacity of 72 mAh g^{-1}, which increases to 89 mAh g^{-1} by the 20th cycle. After 250 cycles, the capacity stabilizes at 85 mAh g^{-1}, indicating only a 4.5% capacity loss. Upon increasing the PEDOT:PSS content to 10 wt% (Figure 2d), the electrochemical behavior remains similar to that of the 7.5 wt% PEDOT:PSS electrode. The discharge capacity reaches a maximum of 86 mAh g^{-1} after 20 cycles and gradually decreases to 78 mAh g^{-1} by 250th cycle, corresponding to a 9.3% capacity loss.

Overall, these findings suggest a slight deviation from the charge–discharge mechanism reported by Kolek et al.[15,29,30] Instead of exhibiting a high initial capacity followed by a decrease and recovery, the PEDOT:PSS containing electrodes demonstrate a lower initial discharge capacity. This variation in the behavior can be linked to the microstructural changes in the electrode resulting from processing with PEDOT:PSS, since PVMPT and CB-only electrodes display a trend more consistent with the previous reports. Another plausible explanation is that PEDOT:PSS tends to form a thin film on the electrode surface when used in electrode paste preparation,[21] which could hinder

© 2025 The Author(s). Advanced Energy and Sustainability Research published by Wiley-VCH GmbH

26999412, 2026, 3, Downloaded from https://advanced.onlinelibrary.wiley.com/doi/10.1002/aesr.202500428 by Karlsruher Institut Fur Technologie, Wiley Online Library on [01/11/2026]. See the Terms and Conditions (https://onlinelibrary.wiley.com/terms-and-conditions) on Wiley Online Library for rules of use; OA articles are governed by the applicable Creative Commons License

ion transport, accounting for the initial low capacity. With further cycling, the PVMPT active sites may gradually become more accessible to anions, leading to the observed increase in capacity during the early stages of cycling. After ≈20 cycles, the capacity stabilizes, suggesting that maximum accessibility of the active sites is achieved at this point.

Figures 3a–d presents differential specific capacity versus potential plots for electrodes containing different amounts of PEDOT:PSS, derived from their corresponding potential versus capacity curves. These plots provide valuable insights into the electrochemical behavior and cycling performance of the cells. Figure 3a displays the differential capacity plot for electrodes without PEDOT:PSS (0 wt%). The initial oxidation (charge) peak appears at 3.59 V versus Li|Li^+, and the corresponding reduction (discharge) peak is at ≈3.53 V versus Li|Li^+. Throughout cycling (20th, 100th, and 200th), the oxidation peak remains relatively stable at ≈3.54 V versus Li|Li^+, with the reduction peak consistently at 3.53 V versus Li|Li^+. By the 250th cycle, a slight increase in oxidation potential to 3.55 V versus Li|Li^+, and reduced peak intensity indicate a gradual decline in accessible capacity. In Figure 3b (5 wt% PEDOT:PSS), the initial oxidation and reduction peaks are at 3.59 V versus Li|Li^+ and 3.52 V versus Li|Li^+, respectively. By the 20th cycle, these slightly shift to 3.54 V versus Li|Li^+ (oxidation) and 3.51 V versus Li|Li^+ (reduction), maintaining similar values up to the 100th cycle. At the 250th cycle, oxidation remains at 3.54 V versus Li|Li^+, while reduction shifts slightly to 3.50 V versus Li|Li^+. Figure 3c shows the 7.5 wt% PEDOT:PSS electrode behavior, where the initial oxidation peak is at 3.59 V versus Li|Li^+ and reduction at 3.53 V versus Li|Li^+. Over cycling, oxidation gradually shifts to 3.53 V versus Li|Li^+ (20th cycle) and 3.52 V versus Li|Li^+ (100th to 250th cycle), while the reduction peak remains steady around 3.52 V versus Li|Li^+. Figure 3d, corresponding to the 10 wt% PEDOT:PSS electrodes, reveals an initial oxidation at 3.59 V versus Li|Li^+ and reduction at 3.52 V versus Li|Li^+. By the 20th cycle, oxidation shifts to 3.54 V versus Li|Li^+, with reduction unchanged. A gradual drift in redox potentials and a reduction in peak intensity are observed with further cycling.

All PEDOT:PSS-containing electrodes exhibit good redox reversibility, with only minor shifts in peak potentials over time. The overall peak shapes remain consistent, indicating the electrochemical stability of PVMPT over prolonged cycling. However, oxidation peak broadening is observed, likely due to anion insertion and de-insertion result in the structural rearrangements of the polymer and microstructural changes in the electrode.

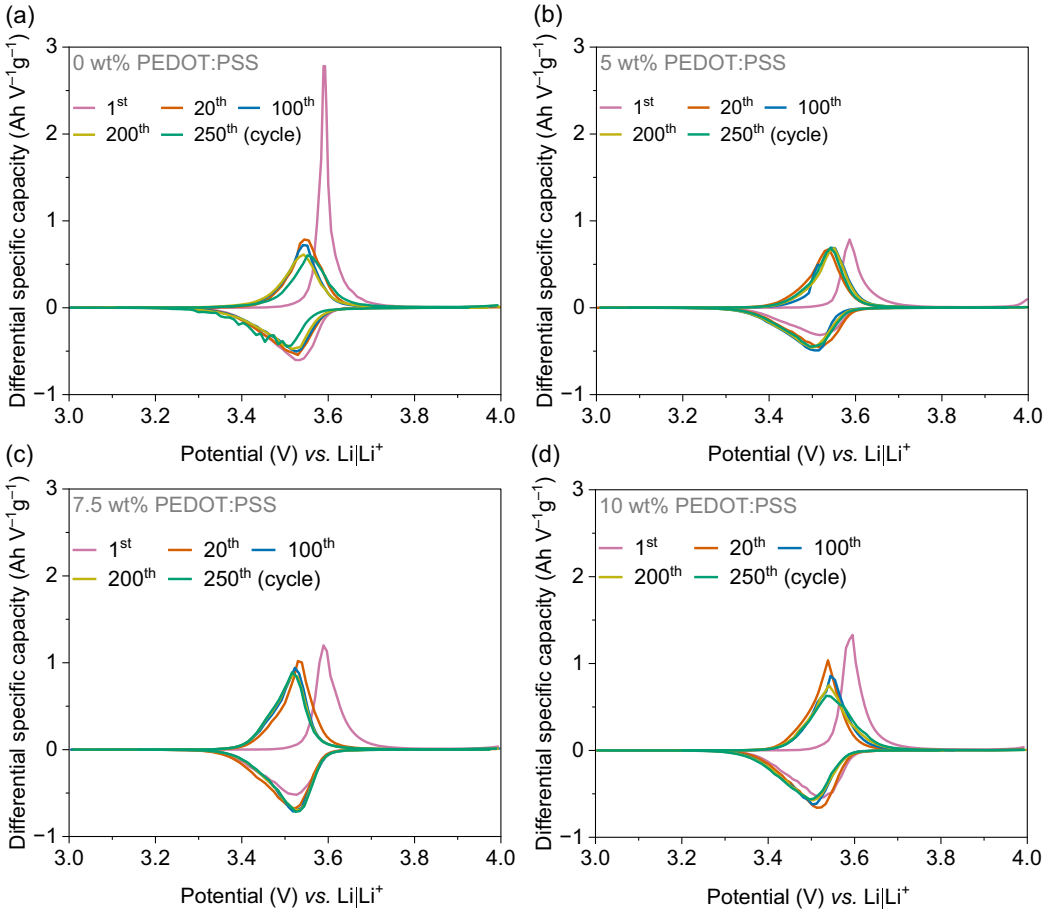


Figure 3. Differential specific capacity versus potential plots for selected cycles of cells operated at a 1C rate, comparing electrodes without PEDOT:PSS to those containing PEDOT:PSS at three different weight percentages: a) 0 wt% PEDOT:PSS, b) 5 wt% PEDOT:PSS, c) 7.5 wt% PEDOT:PSS, and d) 10 wt% PEDOT:PSS.

© 2025 The Author(s). Advanced Energy and Sustainability Research published by Wiley-VCH GmbH

26999412, 2026, 3, Downloaded from https://advanced.onlinelibrary.wiley.com/doi/10.1002/aesr.202500428 by Karlsruher Institut Fur Technologie, Wiley Online Library on [01/11/2026]. See the Terms and Conditions (https://onlinelibrary.wiley.com/terms-and-conditions) on Wiley Online Library for rules of use; OA articles are governed by the applicable Creative Commons License

Figure 4 presents the cross-sectional SEM images and corresponding EDS mappings of electrodes fabricated with varying PEDOT:PSS content. At 0 wt% PEDOT:PSS, the SEM image reveals a highly porous and loosely packed structure, with large voids and poor interconnectivity between the CB-CMC matrix and PVMPT (Figure 4a). This morphology is further supported by the EDS map, which shows an uneven elemental distribution (Figure 4e).

As PEDOT:PSS content increases, the electrode microstructure becomes denser, and connectivity between the CB-PEDOT:PSS-CMC matrix and PVMPT improves. At 5 wt% PEDOT:PSS, the electrode appears more compact, with enhanced interconnectivity and reduced pore size (Figure 4b). The corresponding EDS map indicates a more uniform distribution of elements compared to the 0 wt% PEDOT:PSS sample (Figure 4f). At 7.5 wt% PEDOT:PSS, the electrode exhibits an optimal microstructure characterized by dense packing, uniform elemental distribution, and strong interfacial contact between the CB-PEDOT:PSS-CMC matrix and PVMPT (Figure 4c). This is evidenced by the EDS map, which shows consistent elemental uniformity (Figure 4g). However, increasing the PEDOT:PSS content to 10 wt% results in an overly dense structure with reduced porosity and visible voids (Figure 4d). The EDS mapping (Figure 4h) reveals slight nonuniformity in element distribution, suggesting that these voids may disrupt the formation of a uniform conductive network, thereby hindering efficient charge or ion transport.

Additionally, particle cracking is observed (indicated by arrows), likely caused by densification at 3 tons of pressure. Due to the lower carbon content in these formulations, PVMPT is more exposed on the electrode surface. This contrasts with electrodes densified at 3 tons containing 45 wt% carbon, where the material is entirely wrapped, helping to shield it from direct mechanical stress (Figure S1, Supporting Information). Overall, the combined SEM and EDS analyses indicate that a PEDOT:PSS content of 7.5 wt% provides the best balance between structural integrity and uniform active material distribution. This composition appears to be the most promising for optimizing the performance of PVMPT-based composite electrodes.

In contrast, the surface SEM images show that increasing the PEDOT:PSS content leads to a reduced dispersion quality, with some regions exposing the current collector and binder particles, as highlighted by yellow boxes and arrows, indicating poor dispersion and agglomeration. (**Figures 5**b–d) which is not observed in 0 wt% PEDOT:PSS electrodes (Figure 5a). Although the PEDOT:PSS:CB:CMC mixture was initially well-dispersed, the addition of PVMPT disrupted this uniformity as observed during electrode paste preparation, likely due to unfavorable surface interactions within the paste, resulting in the nonuniform morphologies in few areas as seen in Figures 5b–d. Despite this inhomogeneity, both PEDOT:PSS and CB are still observed in specific regions forming a continuous conductive network, which positively contributes to the electrochemical performance. It is also evident that the surface of the PVMPT particles appears smoother in the PEDOT:PSS-containing electrodes, whereas a rougher particle surface is observed in electrodes without PEDOT:PSS. This suggests that PEDOT:PSS likely coats the

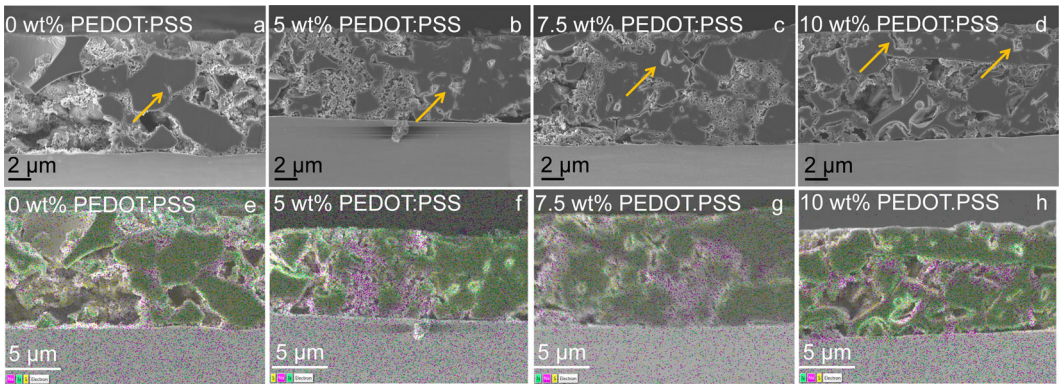


Figure 4. Cross-sectional SEM images along with corresponding EDS elemental mapping of electrodes prepared without PEDOT:PSS and with different PEDOT:PSS weight ratios, maintaining 80 wt% PVMPT content. The images correspond to the following compositions: a,e) 0 wt% PEDOT:PSS, b,f) 5 wt% PEDOT:PSS, c,g) 7.5 wt% PEDOT:PSS, and d,h) 10 wt% PEDOT:PSS. Elemental distributions are color-coded as follows: Nitrogen (N) in green from PVMPT, sodium (Na) in magenta from CMC, and sulfur (S) in yellow from PVMPT and PEDOT:PSS.

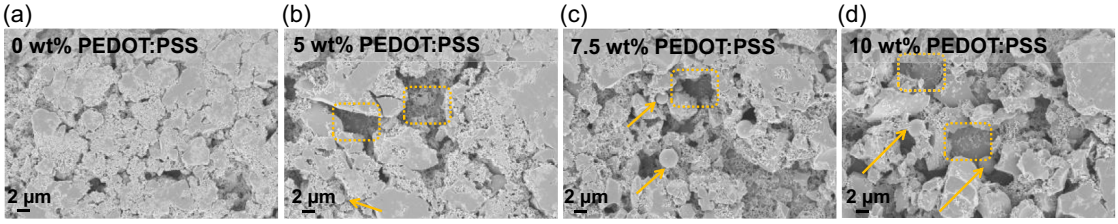


Figure 5. Top-view SEM images of electrodes prepared without PEDOT:PSS and with varying PEDOT:PSS weight ratios, maintaining 80 wt% PVMPT: a) 0 wt% PEDOT:PSS, b) 5 wt% PEDOT:PSS, c) 7.5 wt% PEDOT:PSS, and d) 10 wt% PEDOT:PSS, respectively.

© 2025 The Author(s). Advanced Energy and Sustainability Research published by Wiley-VCH GmbH

26999412, 2026, 3, Downloaded from https://advanced.onlinelibrary.wiley.com/doi/10.1002/aesr.202500428 by Karlsruher Institut Fur Technologie, Wiley Online Library on [01/11/2026]. See the Terms and Conditions (https://onlinelibrary.wiley.com/terms-and-conditions) on Wiley Online Library for rules of use; OA articles are governed by the applicable Creative Commons License

surface of the PVMPT particles, potentially leading to an enhanced conductivity.

Figure 6a presents the long-term cycling stability plot (averaged plot) of electrodes prepared with 80 wt% PVMPT, 5 wt% CMC, and varying PEDOT:PSS and CB weight ratios cycled at a 1C rate over 250 cycles. The charge–discharge performance and Coulombic efficiency over extended cycling are depicted in Figure S2, Supporting Information. The electrode without PEDOT:PSS (0 wt% PEDOT:PSS) exhibited a maximum discharge capacity of 64 mAh g^{-1}, corresponding to 57% of the theoretical capacity. Adding 5 wt% PEDOT:PSS slightly reduced the maximum discharge capacity to 60 mAh g^{-1}. However, increasing the PEDOT:PSS content to 7.5 wt% and 10 wt% improved the discharge capacity to 84 and 80 mAh g^{-1}, corresponding to 75% and 71% of the theoretical capacity, respectively.

It is evident that a small amount of PEDOT:PSS does not enhance the accessible capacity. However, increasing the PEDOT:PSS content leads to a notable improvement, with the maximum discharge capacity reaching ≈ 80mAh g^{-1}. The highest discharge capacity observed for an electrode with 50 wt% PVMPT, 45 wt% CB, and 5 wt% CMC binder was 104 mAh g^{-1} (Figure S3, Supporting Information). When PEDOT:PSS was introduced, the total carbon content in the electrode decreased to 15 wt%, and PEDOT:PSS acted as both a conductive additive and a binder, which enhanced the conductivity as well as adhesion, resulting in a maximum discharge capacity of 84 mAh g^{-1}, which is equivalent to 81% of the capacity achieved with 45 wt% CB (Figure S3, Supporting Information). Regardless of the weight ratio, all formulations demonstrated excellent capacity retention. The difference between the charge and discharge voltages, referred to as voltage hysteresis (ΔV), arises from internal resistance, side reactions, or degradation processes during cycling. **Figure 6**b presents the ΔV plot over 250 cycles at a 1C rate. Electrodes with 0 wt% PEDOT:PSS initially exhibit a ΔV of ≈0.11 V, which decreases over the first 50 cycles but then increases again to about 0.07 V by 200th cycle. After 200 cycles, ΔV rises back to around 0.11 V, indicating a gradual increase in resistance. In contrast, 5 wt% PEDOT:PSS electrodes begin with a higher ΔV (≈0.2 V) in the first cycle, which rapidly decreases to 0.05 V within the first few cycles. However, ΔV gradually increases to around 0.08 V as cycling continues. Electrodes containing 7.5 wt% and 10 wt% PEDOT:PSS initially show higher hysteresis values of ≈0.13 V, but this quickly decreases to about 0.06 V within the first 50 cycles. Over long-term cycling, the 7.5 wt% PEDOT:PSS electrodes exhibit a lower and more stable ΔV of ≈0.04 V, while the 10 wt% PEDOT:PSS electrodes maintain a ΔV of ≈0.06 V, both indicating relatively lower internal resistance. These results clearly demonstrate that incorporating PEDOT:PSS at an optimal concentration can reduce voltage hysteresis, thereby lowering cell resistance. Among the samples, the 7.5 wt% PEDOT:PSS electrode (with an equal weight ratio of PEDOT:PSS and CB) delivers the lowest and most stable ΔV throughout cycling, suggesting enhanced conductivity and reduced resistance. Higher ΔV values, as observed in the 0 wt% PEDOT:PSS electrodes after 200 cycles, are associated with increased resistance. While the 10 wt% PEDOT:PSS electrodes also show improved performance, the 7.5 wt% PEDOT:PSS composition appears to be the optimal concentration for achieving enhanced electrochemical performance.

Furthermore, the rate performance of PEDOT:PSS-containing electrodes was evaluated over a wide C-rate range, from 1C up to 100C, and compared against the 0 wt% PEDOT:PSS electrode. **Figure 7**a presents the average rate capability plot, highlighting the performance differences between the 0 wt% PEDOT:PSS electrode and those containing varying PEDOT:PSS weight percentages. Prior to rate testing, all cells underwent a pre-cycling phase at 1C for 20 cycles, which also serves as an activation period. Following this, the C-rate was gradually increased to 100C and subsequently decreased back to 1C. The comparative long-term stability plot and complete rate performance plot, along with the corresponding standard deviation plots, are provided in Figure S4, Supporting Information. As expected, increasing the C-rate led to a decrease in accessible discharge capacity. Interestingly, when the C-rate was reversed back to 1C, a slight recovery in capacity was observed for higher C-rates, indicating good polymer accessibility for anions and suggesting that no irreversible side reactions occurred during the high-rate cycling. This is further evidenced by the differential specific

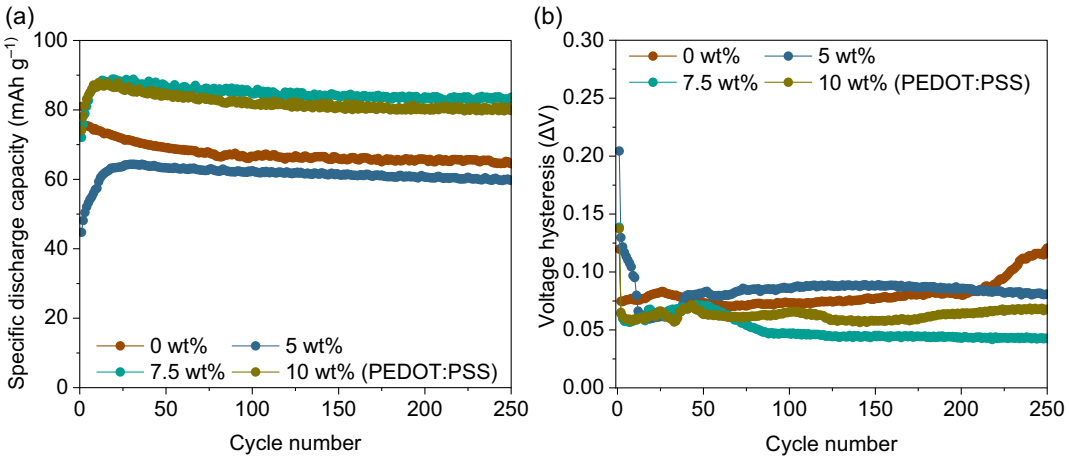


Figure 6. a) Galvanostatic cycling measurements showing long-term cycling stability (averaged value of the specific discharge capacity); b) voltage hysteresis (ΔV) versus cycle number plot (averaged) of the electrodes cycled at a 1C rate for 250 cycles.

© 2025 The Author(s). Advanced Energy and Sustainability Research published by Wiley-VCH GmbH

26999412, 2026, 3, Downloaded from https://advanced.onlinelibrary.wiley.com/doi/10.1002/aesr.202500428 by Karlsruher Institut Fur Technologie, Wiley Online Library on [01/11/2026]. See the Terms and Conditions (https://onlinelibrary.wiley.com/terms-and-conditions) on Wiley Online Library for rules of use; OA articles are governed by the applicable Creative Commons License

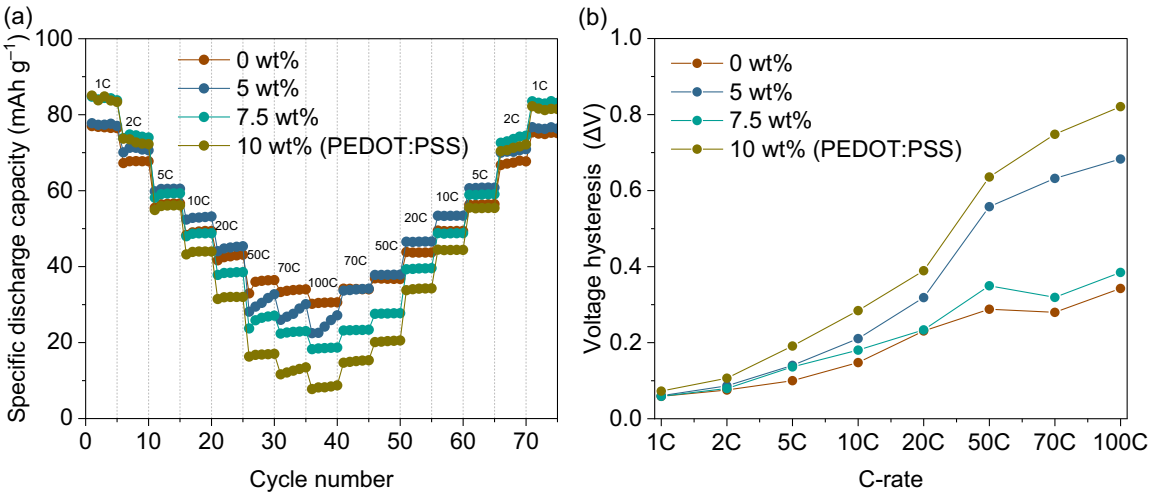


Figure 7. a) Averaged rate capability plots over 75 cycles and b) voltage hysteresis (ΔV) versus cycle number plot cycled at various C-rates, obtained from the rate capability test.

capacity versus potential plots obtained from C-rate evaluations, as shown in Figure S5, Supporting Information, which illustrates good reversibility and confirms the electrochemical stability of the polymer. Notably, the 0 and 5 wt% PEDOT:PSS electrodes demonstrated superior rate capability, delivering higher discharge capacities even at elevated C-rates compared to the 7.5 and 10 wt% PEDOT:PSS electrodes. The data clearly show that increasing the PEDOT:PSS content results in a reduction in accessible discharge capacity, when comparing the 0 and 5 wt% PEDOT:PSS electrodes. This observation contradicts the findings of Ma et al. where enhanced rate performance was reported for DTT electrodes coated with PEDOT:PSS.[17] This discrepancy can be explained by differences in material preparation. In the cited work, PEDOT:PSS was coated directly onto the active material (DTT), resulting in a more uniform conductive network. Additionally, the paste preparation was employed NMP as the solvent. In contrast, herein, PEDOT:PSS is used as a conductive additive rather than a coating, and the poor water solubility of PVMPT results in inadequate dispersion as evidenced by the surface SEM morphology (Figure 5), which may contribute to the reduced performance observed at higher C-rate.

Figure 7b shows the ΔV plot obtained at various C-rates as obtained from the rate capability measurements. The corresponding potential versus capacity profiles are provided in Figure S6, Supporting Information. As seen in Figure 7b, ΔV increases with increase in C-rates, indicating higher voltage loss at higher (dis)charge rates, which is associated with higher polarization and internal resistance. All the electrodes exhibit a ΔV below 0.4 V up to 20 C. However, at higher C-rates (50C to 100C), ΔV rises, reaching 0.82 V for 10 wt% PEDOT:PSS electrodes and 0.68 V for 5 wt% PEDOT:PSS electrodes at 100C. These values are relatively higher compared to 0 wt% PEDOT:PSS (0.34 V) and 7.5 wt% PEDOT:PSS electrodes (0.38 V) indicating relatively higher resistance at higher C-rates for the former. Notably, both the 0 wt% PEDOT:PSS and 7.5 wt% PEDOT:PSS electrodes maintain ΔV below <0.4 V across the entire C-rate range investigated, suggesting lower polarization loss. In contrast, the higher ΔV values observed in the 5 wt% PEDOT:PSS and 10 wt% PEDOT:PSS electrodes at elevated C-rates point to inferior rate performance, likely due to increased resistance.

Overall, the inclusion of 7.5 wt% PEDOT:PSS achieves the most optimal balance, demonstrating low cell resistance, minimal ΔV, and high discharge capacity at 1C, along with optimal performance at higher C-rates.

4.2. Charge Storage Kinetics of the PVMPT Electrodes

To analyze the electrochemical kinetics of PVMPT electrodes, cyclic voltammetry (CV) was performed at different scan rates ranging from 0.1 to 10 mV s^{-1}. The typical cyclic voltammograms (CVs) for PVMPT composite electrode processed with and without PEDOT:PSS at various scan rates are shown in Figure S7, Supporting Information. The oxidative and reductive peaks represent the anion (PF_6^-) insertion (charge) and de-insertion (discharge). The area under the CV curve represents the total charge stored, which consists of two processes: a Faradaic contribution from ion insertion and charge transfer with surface atoms (pseudocapacitance) and the non-Faradaic contribution from the double layer effect.[33]

From the scan-rate dependent CVs, it is evident that the peak currents (i) increase with scan rate (ν). The measured current follows the power-law relationship with scan rate (ν), expressed as $i = a\nu^b$, where a and b are adjustable parameters. The b-value is obtained from the slope of log i versus log ν plot. A b-value of 0.5 indicates a diffusion-controlled redox processes while a b-value of 1 indicates a surface-dominant redox processes.[33–35] As shown in **Figure 8**a, for the 0 wt% PEDOT:PSS electrodes, the b values are 0.715 ± 0.026 (charge sweep) and 0.641 ± 0.016 (discharge sweep), indicating a mixed behavior with a tendency toward surface-controlled reactions. For the 5 wt% PEDOT:PSS electrodes (Figure 8b), the b-value increases to 0.8 ± 0.04 (charging) and 0.75 ± 0.01 (discharging), suggesting a more surface-controlled

© 2025 The Author(s). Advanced Energy and Sustainability Research published by Wiley-VCH GmbH

26999412, 2026, 3, Downloaded from https://advanced.onlinelibrary.wiley.com/doi/10.1002/aesr.202500428 by Karlsruher Institut Fur Technologie, Wiley Online Library on [01/11/2026]. See the Terms and Conditions (https://onlinelibrary.wiley.com/terms-and-conditions) on Wiley Online Library for rules of use; OA articles are governed by the applicable Creative Commons License

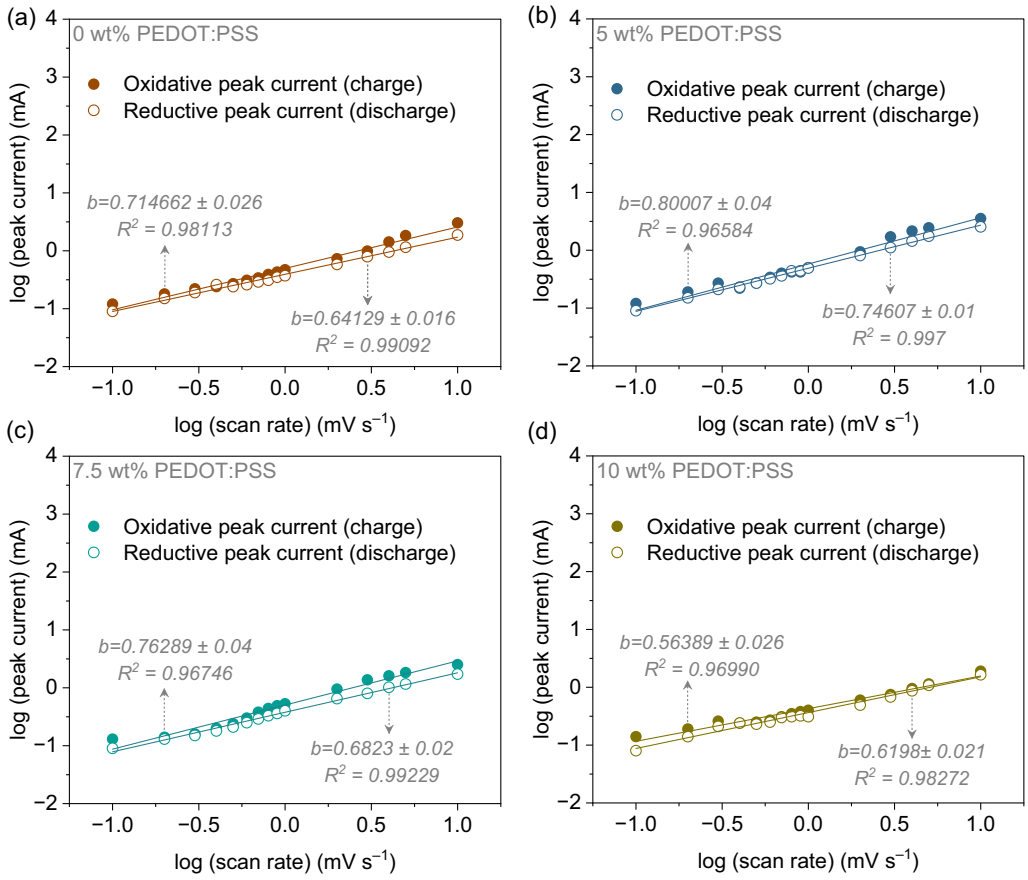


Figure 8. Determination of the *b*-value from the peak currents for a) 0 wt% PEDOT:PSS, b) 5 wt% PEDOT:PSS, c) 7.5 wt% PEDOT:PSS, and d)10 wt% PEDOT:PSS electrodes at different scan rates.

storage mechanism. However, with further increase in PEDOT:PSS content to 7.5 and 10 wt%, (Figures 8c,d), the *b*-values decrease to 0.763 ± 0.04 (charging), 0.682 ± 0.02 (discharging) and 0.564 ± 0.026 (charging), and 0.62 ± 0.02 (discharging), respectively, indicating a shift toward more diffusion-controlled charge storage. Overall, these results suggest that the electrochemical reaction in PVMPT electrodes is primarily governed by surface-controlled mechanisms, with increasing diffusion contributions at higher PEDOT:PSS content.

5. Conclusion

This study systematically investigates the effect of incorporating PEDOT:PSS into PVMPT-based electrodes to develop low-carbon content electrodes with enhanced electrochemical performance. By formulating electrodes with a high active material ratio of 80 wt% PVMPT and varying (PEDOT:PSS):CB ratios, it is demonstrated that PEDOT:PSS plays a dual role as both a conductive additive and a binder, influencing electrode morphology and rate capability. Among the investigated formulations, the electrode containing 7.5 wt% PEDOT:PSS exhibited the most balanced performance, achieving a maximum specific discharge capacity of 84 mAh g^{-1} with a total carbon content of only 15 wt% (CB + PEDOT:PSS) after 250 cycles at 1C rate. Electrode microstructural analysis via SEM and EDS mapping confirmed that 7.5 wt% PEDOT:PSS facilitates a uniform elemental distribution and establishes a well-connected conductive network. However, increasing the PEDOT:PSS content beyond this point introduced challenges such as poor dispersion, inhomogeneity, and reduced porosity, which negatively affected electrode microstructure. Symmetric C-rate testing revealed that electrodes with no or low PEDOT:PSS content (0 and 5 wt%) displayed good rate capability at higher C-rates, while the 7.5 wt% PEDOT:PSS formulation showed superior overall electrochemical characteristics, including higher specific discharge capacity, lower voltage hysteresis, and better structural integrity. Kinetic analysis revealed that the charge storage to a large extend is surface-controlled, with diffusion-controlled processes being more predominant as PEDOT:PSS content increases. These findings suggest that an optimized balance between PEDOT:PSS and CB ensures both good conductivity and structural cohesion in low-carbon electrodes. With further improvements in mixing techniques and formulation optimization, this approach shows strong potential for developing high-performance, sustainable organic battery systems.

Supporting Information

Supporting Information is available from the Wiley Online Library or from the author.

© 2025 The Author(s). Advanced Energy and Sustainability Research published by Wiley-VCH GmbH

26999412, 2026, 3, Downloaded from https://advanced.onlinelibrary.wiley.com/doi/10.1002/aesr.202500428 by Karlsruher Institut Fur Technologie, Wiley Online Library on [01/11/2026]. See the Terms and Conditions (https://onlinelibrary.wiley.com/terms-and-conditions) on Wiley Online Library for rules of use; OA articles are governed by the applicable Creative Commons License

Acknowledgements

The authors S.P.P., P.E., and M.W. gratefully acknowledge the Ministry for Culture and Science of North Rhine-Westphalia (Germany) for supporting this work through the International Graduate School for Battery Chemistry, Characterization, Analysis, Recycling, and Application (BACCARA). The synthesis of PVMPT was carried out as part of the research activities at CELEST (Center for Electrochemical Energy Storage Ulm-Karlsruhe) by P.P. and B.E. with funding provided by the Deutsche Forschungsgemeinschaft (DFG, German Research Foundation) under the following project IDs: 390874152 (POLiS Cluster of Excellence, EXC 2154), 441236036 (SPP 2248: Polymer-based Batteries), 445470598, 445471097, 445471845, and 528773185.

Open Access funding enabled and organized by Projekt DEAL.

Conflict of Interest

The authors declare no conflict of interest.

Data Availability Statement

The data that support the findings of this study are available from the corresponding author upon reasonable request.

Keywords

lithium-organic battery, low-carbon content, PEDOT:PSS, PVMPT electrode

Received: October 15, 2025
Revised: November 6, 2025
Published online:

[1] K. Turcheniuk, D. Bondarev, G. G. Amatucci, G. Yushin, *Mater. Today* **2021**, *42*, 57.
[2] A. El Kharbachi, O. Zavorotynska, M. Latroche, F. Cuevas, V. Yartys, M. Fichtner, *J. Alloys. Comp.* **2020**, *817*, 153261.
[3] J. Santillán-Saldivar, T. Gaugler, C. Helbig, A. Rathgeber, G. Sonnemann, A. Thorenz, A. Tuma, *J. Ind. Ecol.* **2021**, *25*, 1051.
[4] A. Zeng, W. Chen, K. D. Rasmussen, X. Zhu, M. Lundhaug, D. B. Müller, J. Tan, J. K. Keiding, L. Liu, T. Dai, A. Wang, G. Liu, *Nat. Commun.*. **2022**, *13*, 1341.
[5] Y. Lu, J. Chen, *Nat. Rev. Chem.* **2020**, *4*, 127.
[6] M. Armand, J.-M. Tarascon, *Nature* **2008**, *451*, 652.
[7] D. Larcher, J.-M. Tarascon, *Nat. Chem.* **2015**, *7*, 19.
[8] P. Poizot, J. Gaubicher, S. Renault, L. Dubois, Y. Liang, Y. Yao, *Chem. Rev.* **2020**, *120*, 6490.
[9] R. Wessling, P. Penert, B. Esser, *Adv. Energy Mater.* **2025**, *15*, 2500150.
[10] B. Esser, F. Dolhem, M. Becuwe, P. Poizot, A. Vlad, D. Brandell, *J. Power Sources* **2021**, *482*, 228814.
[11] P. Poizot, F. Dolhem, J. Gaubicher, *Curr. Opin. Electrochem.* **2018**, *9*, 70.
[12] S. Dühnen, J. Betz, M. Kolek, R. Schmuch, M. Winter, T. Placke, *Small Methods* **2020**, *4*, 2000039.
[13] B. Esser, *Org. Mater.* **2019**, *1*, 63.
[14] Y. Lu, Q. Zhang, L. Li, Z. Niu, J. Chen, *Chem* **2018**, *4*, 2786.
[15] V. Perner, D. Diddens, F. Otteny, V. Küpers, P. Bieker, B. Esser, M. Winter, M. Kolek, *ACS Appl. Mater. Interfaces* **2021**, *13*, 12442.
[16] B. Tengen, T. Winkelmann, N. Ortlieb, V. Perner, G. Studer, M. Winter, B. Esser, A. Fischer, P. Bieker, *Adv. Funct. Mater.* **2023**, *33*, 2210512.
[17] T. Ma, Q. Zhao, J. Wang, Z. Pan, J. Chen, *Angew. Chem., Int. Ed.,* **2016**, *55*, 6428.
[18] M. Lee, J. Hong, H. Kim, H.-D. Lim, S. B. Cho, K. Kang, C. B. Park, *Adv. Mater.* **2014**, *26*, 2558.
[19] A. Molina, N. Patil, E. Ventosa, M. Liras, J. Palma, R. Marcilla, *ACS Energy Lett.* **2020**, *5*, 2945.
[20] A. Innocenti, I. Á. Moisés, O. Lužanin, J. Bitenc, J.-F. Gohy, S. Passerini, *ACS Appl. Mater. Interfaces* **2024**, *16*, 48757.
[21] M. Grygiel, M. Ratyński, A. Czerwiński, B. Hamankiewicz, *Appl. Phys. A* **2024**, *130*, 08039.
[22] T. M. Higgins, S.-H. Park, P. J. King, C. J. Zhang, N. McEvoy, N. C. Berner, D. Daly, A. Shmeliov, U. Khan, G. Duesberg, V. Nicolosi, J. N. Coleman, *ACS Nano* **2016**, *10*, 3702.
[23] P. R. Das, L. Komsiyska, O. Osters, G. Wittstock, *ECS Trans.* **2015**, *68*, 45.
[24] K. Sun, S. Zhang, P. Li, Y. Xia, X. Zhang, D. Du, F. H. Isikgor, J. Ouyang, *J. Mater. Sci.- Mater. Electron.* **2015**, *26*, 4438.
[25] M. Goyal, S. N. Agarwal, K. Singh, N. Bhatnagar, *J. Appl. Polym. Sci.* **2023**, *140*, 53830.
[26] N. Yuca, I. Kalafat, O. S. Taskin, E. Aric, *Polym. Adv. Technol.* **2023**, *34*, 279.
[27] S. N. Eliseeva, O. V. Levin, E. G. Tolstopjatova, E. V. Alekseeva, R. V. Apraksin, V. V. Kondratiev, *Mater. Lett.* **2015**, *161*, 117.
[28] M. Kato, H. Sano, T. Kiyobayashi, N. Takeichi, M. Yao, *ACS Omega* **2020**, *5*, 18565.
[29] M. Kolek, F. Otteny, P. Schmidt, C. Mück-Lichtenfeld, C. Einholz, J. Becking, E. Schleicher, M. Winter, P. Bieker, B. Esser, *Energy Environ. Sci.* **2017**, *10*, 2334.
[30] M. Kolek, F. Otteny, J. Becking, M. Winter, B. Esser, P. Bieker, *Chem. Mater.* **2018**, *30*, 6307.
[31] B. Esser, I. H. Morhenn, M. Keis, *Acc. Mater. Res.* **2025**, *6*, 754.
[32] N. Ortlieb, B. Tengen, V. Perner, M. Winter, B. Esser, P. Bieker, A. Fischer, *Adv. Funct. Mater.* **2025**, *33*, 2422302.
[33] J. Wang, J. Polleux, J. Lim, B. Dunn, *J. Phys. Chem. C* **2007**, *111*, 14925.
[34] H. Lindström, S. Södergren, A. Solbrand, H. Rensmo, J. Hjelm, A. Hagfeldt, S.-E. Lindquist, *J. Phys. Chem. B* **1997**, *101*, 7717.
[35] V. Augustyn, J. Come, M. A. Lowe, J. W. Kim, P.-L. Taberna, S. H. Tolbert, H.-D. Abruña, P. Simon, B. Dunn, *Nat. Mater.* **2013**, *12*, 518.

© 2025 The Author(s). Advanced Energy and Sustainability Research published by Wiley-VCH GmbH

26999412, 2026, 3, Downloaded from https://advanced.onlinelibrary.wiley.com/doi/10.1002/aesr.202500428 by Karlsruher Institut Fur Technologie, Wiley Online Library on [01/11/2026]. See the Terms and Conditions (https://onlinelibrary.wiley.com/terms-and-conditions) on Wiley Online Library for rules of use; OA articles are governed by the applicable Creative Commons License